www.MaterialsViews.com

ADVANCED
FUNCTIONAL
MATERIALS
www.afm-journal.de

FULL PAPER

Elastomeric Electronic Skin for Prosthetic Tactile Sensation

Aaron P. Gerratt, Hadrien O. Michaud, and Stéphanie P. Lacour*

This report demonstrates a wearable elastomer-based electronic skin including resistive sensors for monitoring finger articulation and capacitive tactile pressure sensors that register distributed pressure along the entire length of the finger. Pressure sensitivity in the order of 0.001 to 0.01 kPa⁻¹ for pressures from 5 to 405 kPa, which includes much of the range of human physiological sensing, is achieved by implementing soft, compressible silicone foam as the dielectric and stretchable thin-metal films. Integrating these sensors in a textile glove allows the decoupling of the strain and pressure cross-sensitivity of the tactile sensors, enabling precise grasp analysis. The sensorized glove is implemented in a human-in-the-loop system for controlling the grasp of objects, a critical step toward hand prosthesis with integrated sensing capabilities.

1. Introduction

Individuals rely on proprioceptive and cutaneous inputs to maintain normal stance and accomplish fundamental activities of daily life.[1] Strategies to help understand and then reconstruct and restore the sense of touch are needed for areas as diverse as human haptic perception,[2] robotic manipulation,[3] control of a prosthetic limb,[4] aging,[5] clinical rehabilitation therapies following traumatic injuries,[6] and neurodegenerative diseases.[7] Touch differs from the other senses in that it spreads over the entire body. Tactile perception integrates sensory information from the skin, joints, tendons, and muscles. When grasping objects, proprioceptors report on the orientation of the hand and fingers while skin mechanoreceptors sense hardness and texture of the objects. In addition, skin thermoreceptors encode absolute and relative change in temperature of handled objects, and nociceptors provide alerts on harmful stimuli and interactions.

The last few years have seen a dramatic increase in the number of academic research efforts to design and fabricate large-area sensory electronic skins, called e-skins, mimicking human skin perceptive functions, and full body coverage[8,9] or implementing nearly imperceptible health monitors.[10–12] Remarkable sensitivities on the order of 1 Pa⁻¹ to 100 kPa⁻¹ have been demonstrated across varied pressure ranges in flexible sensors (0.001 Pa to 10 kPa,[13–15] 0.01 to 10 kPa,[16,17] and 0.1 to 100 kPa)[18] and stretchable sensors (0.1 to 100 kPa).[19,20]

Dr. A. P. Gerratt, H. O. Michaud, Prof. S. P. Lacour
École Polytechnique Fédérale de Lausanne
Laboratory for Soft Bioelectronic Interfaces,
Center for Neuroprosthetics
1015 Lausanne, Switzerland
E-mail: stephanie.lacour@epfl.ch

Human skin is capable of transducing pressures in the range of 100 Pa (light touch) to 1 MPa (full body weight bearing); common tasks such as object manipulation develop contact pressures on the order of 10 kPa.[21,22] Moreover, sensitivity of human skin to applied pressures is complex and varies widely by type of mechanoreceptor and type of stimulation (normal pressure, shear pressure, frequency, magnitude).[23]

Although distributed sensing using arrays of thin-film transistors on ultrathin plastic foils combined with soft mechanical sensors has also been demonstrated,[11,24–26] most reported skin-like sensors are discrete elements. An unmet demand for truly wearable e-skin is mechanical compliance. Natural skin is soft and elastic. Electronic skins should therefore wrap over the external surface of the body and accompany movement, in particular over joints and articulations. To date, pressure sensing data gloves and tactile skins are mainly prepared with flexible polymers[27–29] and conductive textiles.[30,31] These constructs conform well to developable surfaces (e.g., the arm and finger phalanges) but wrinkle and often fail when placed over articulations (e.g., the elbow and finger joints).[32] E-skins prepared entirely with stretchable materials appear as a necessary starting point. Over the last decade, multiple designs of stretchable tactile sensors using elastomers, thin films, composites,[19,33] and conductive liquids[34–36] have been reported, but their systematic characterization in real-life conditions is often incomplete. Stretchable strain sensors are often demonstrated in complex real-life scenarios,[37,38] but in the literature related to stretchable tactile sensors, demonstrations involving dynamic states where bending and stretching of the sensors occur simultaneously are not common, likely due to the challenges of removing cross-sensitivities to strain and noise received from the body. [19,20,39]

In this paper, we report on a stretchable e-skin designed to be worn over the hand, monitor live finger movement, and register distributed pressure along the entire length of the finger. The sensory skin is thin and made entirely of elastic materials, thereby can be mounted on a glove and worn without impeding hand movement (**Figure 1**). The read-out electronics are integrated in a small printed circuit board (PCB) located immediately at the base of each finger. Capacitive pressure sensors combine stretchable gold thin-film electrodes with porous silicone foam (Figure 1a) and display high sensitivity across much of the large dynamic pressure range of human skin. Six adjacent pressure sensors cover the entire length of the finger; two soft metallic shielding layers eliminate noise and cross-sensitivity over the skin and enable multi-touch with
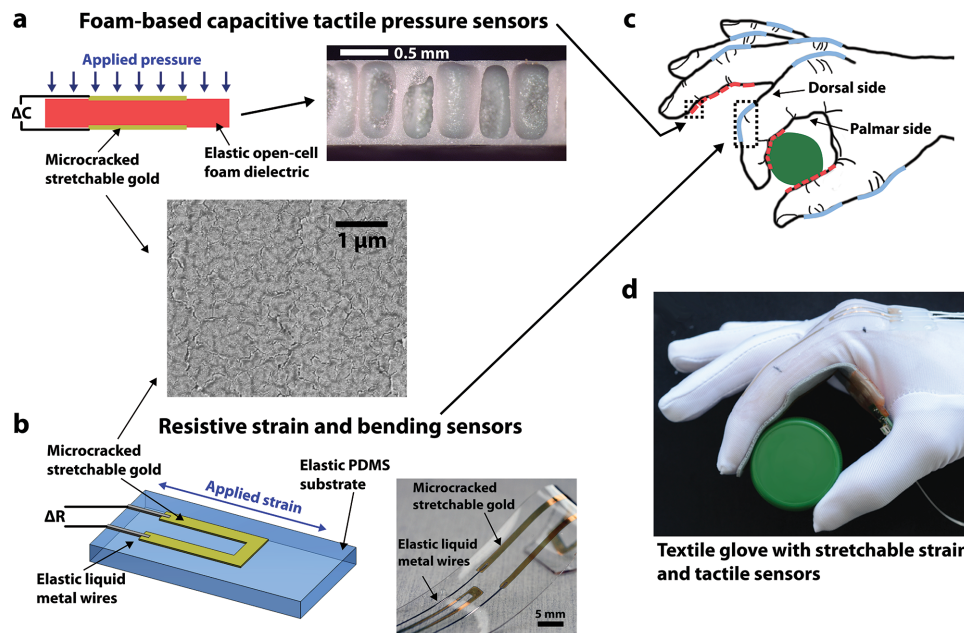
Figure 1. Schematic of the stretchable a) capacitive pressure sensors and b) resistive strain and bending sensors. c) Conceptual drawing of the strain sensors mounted on the dorsal (back) side of fingers to provide bending state information and the pressure sensors on the palmar (grasping) side of fingers to provide grasping pressure information. d) Image of an object being grasped with the fabricated sensors mounted on a textile glove.

plastic or metallic objects. Pressure sensitivities on the order of 0.001 kPa^{-1} are obtained across compressive pressure in the 10 to 405 kPa range, even when the skin is stretched by tens of percent. Resistive strain sensors (Figure 1b) are prepared with high-strain-sensitive stretchable gold thin-film interconnected with printed elastic liquid metal wires. The discrete, soft strain gauges monitor the bending state of two joints of the finger. Their outputs provide proprioceptive-like information but are also used to compensate for the inherent strain-pressure cross-sensitivity of the elastomeric pressure sensors. We demonstrate a glove-like system where pressure sensors are distributed along the palmar (grasping) side of a finger and strain sensors along the dorsal (back) side of a finger (Figure 1c,d). The glove is successfully used in grasping and manipulation tasks, one of which implements the prosthetic sensors in a human-in-the-loop system with visual feedback.

2. Results

2.1. Mechanical Characterization of Elastomeric Materials

We selected a capacitor design for the pressure sensor implementing the elastomer as a soft dielectric material. Parallel plate capacitive sensors present a capacitance C described as $C = \varepsilon_0 \varepsilon A/t$, where ε_0, ε, A, and t are the vacuum permittivity, the relative permittivity of the dielectric material, the sensor electrodes surface area, and the dielectric material thickness, respectively. For a given applied pressure on the sensor, the sensitivity, i.e., the normalized change in capacitance per unit pressure, depends on the compressibility of the dielectric material. We systematically compared the mechanical stress–strain relationships of a range of soft dielectrics (**Figure 2**): two common

bulk silicone elastomers (poly(dimethylsiloxane) (PDMS) and Ecoflex 00-10) and two elastomeric foams (polyurethane Poron 4701 and silicone Bisco HT800). Bulk elastomers (e.g., silicone) are incompressible and have a Poisson's ratio ν of about 0.5. Under compressive stress, these materials experience no volumetric change; they expand in the lateral directions when compressed in the axial direction. Foams, and more specifically open-cell foam elastomers, have Poisson's ratio close to zero because change in foam thickness results from air displacement rather than polymer compression.[40]

The compressibility of bulk elastomers and foam elastomers is summarized (Figure 2a). Each material was compressed to 1.1 MPa using three distinct strain rates. Bulk materials show a rapid, nonlinear increase in stress with applied compressive strains. Stress in the foams, however, remained low, with first a region of linear elasticity until approximately 50% compressive strain (Figure 2b), beyond which a steep increase in stress is observed. Elastomeric foams exhibit enhanced compressibility compared to their bulk counterparts. The linear moduli, calculated by dividing 100 kPa by the corresponding strain at that loading, were 0.19 MPa at 53% strain (silicone foam), 0.25 MPa at 41% strain (polyurethane foam), 0.70 MPa at 14% strain (bulk Ecoflex), and 1.2 MPa at 8.1% strain (bulk PDMS).

The exact shape and slope of the stress–strain curves of foams depend on factors including modulus of the bulk material, foam density, and shape and network of connections between the pores within the foam but were found to be independent of the applied strain rate. Upon uniaxial tensile loading to 30% elongation, the stress–strain response of all four materials is linear (Figure 2c), highlighting the large elasticity of both bulk and foam elastomers. We limited the test to 30% strain to match the natural range of elasticity of human skin.[41] Ecoflex exhibits the lowest modulus $E_{Ecoflex}$ of 45 kPa, confirming its
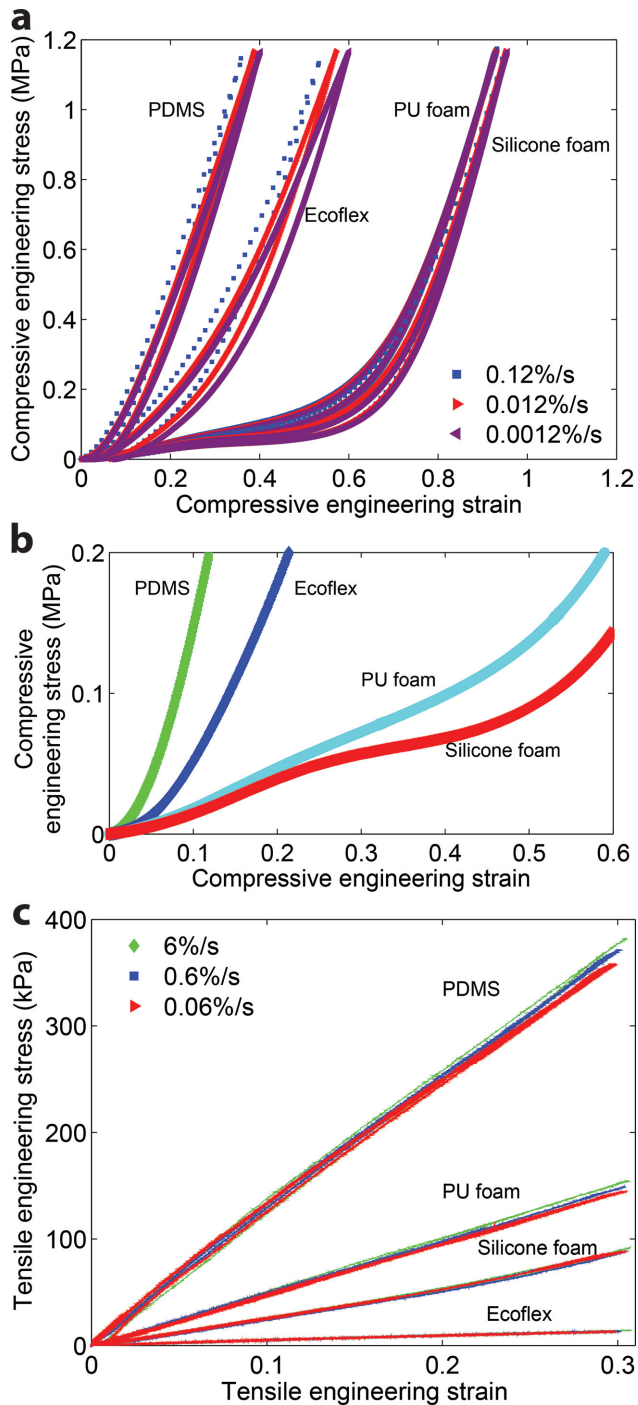
Figure 2. a) Compressive stress–strain curves at three compressive strain rates. b) Close-up on the stress–strain curves recorded at 0.012%/s during extension phase for the four elastomers. c) Tensile stress–strain curves at three tensile strain rates.

large extensibility at low applied mechanical loading;[42] bulk PDMS is the stiffest evaluated elastomer (E_{PDMS} = 1.2 MPa). High compressibility and elasticity prompted us to implement a foam material over a bulk material as the soft dielectric material for skin-like pressure sensors. The silicone foam was chosen over the polyurethane foam because of its slightly

lower modulus and its compatibility with soft microfabrication processing.

2.2. Electromechanical Response of a Silicone Foam-Based Sensor

Figure 3a summarizes the experimental protocol we developed to assess the electromechanical responses of a soft, parallel plate, capacitive sensor prepared with silicone foam dielectric and stretchable thin-metal film electrodes. The 0.88-mm-thick silicone foam is covalently bonded between two 160-µm-thick and metallized PDMS membranes defining electrodes of 1 cm². The soft sensor response, $C(\sigma, \varepsilon_t)$, is evaluated as a function of applied compressive normal pressure σ and applied lateral tensile stretch ε_t. The sensor maintained sensitivity across a large range of applied pressure (5 to 405 kPa) and over demanding strain levels (Figure 3b). We observed a noticeable increase in the capacitance with elongation, a typical side effect in stretchable physical sensors.[19,42] To quantify further this cross-sensitivity, the sensor was compressed to σ = 250 kPa while held stretched at a constant elongation ε_t. The test was repeated for tensile strain levels ranging from ε_t = 0% to 30% in steps of 5% strain. We define the sensors relative capacitance change (Figure 3c) and sensitivity (Figure 3d) as [$C(\sigma, \varepsilon_t)$ − $C(\sigma = 0, \varepsilon_t)$]/$C(0, 0)$ and [$C(\sigma, \varepsilon_t)$ − $C(\sigma = 0, \varepsilon_t)$]/$C(0, 0)/\sigma$, respectively, where $C(\sigma, \varepsilon_t)$ is the measured capacitance, $C(\sigma = 0, \varepsilon_t)$ is the baseline capacitance at the tested tensile strain level ε_t, and $C(0, 0)$ is the initial un-compressed ($\sigma = 0$), un-strained ($\varepsilon_t = 0$) baseline capacitance.

The sensor is robust and reliable across most of the physiological range of mechanical loadings (Figure 3c). The pressure sensitivity at 2 kPa is 0.018 and 0.020 kPa⁻¹ at 0% and 30% applied strain, respectively, and decreases as a negative exponential curve to 0.005 and 0.007 kPa⁻¹ at 0% and 30% applied strain, respectively (Figure 3d). The sensitivity at low pressures is approximately two orders of magnitude higher than that of bulk PDMS and Ecoflex-based pressure sensors.[42–45] As the applied pressure increases, the foam eventually becomes fully compressed and its compressive behavior matches that of the bulk material with sensitivity on the order of 0.001 to 0.0001 kPa⁻¹ (Figure 2a).

Figure 3e displays the sensor response to applied strain and compressive pressure loadings. During testing, tensile strains were first applied and held, and then the compressive pressure was increased. The relative capacitance change linearly increases with the applied tensile strain with increasing sensitivity as the sensor is also compressed. Figure 3f reports the sensor sensitivity to applied strain only, without compressive pressure. Upon stretching, the geometry of the sensor changes: the dielectric thickness decreases and the surface area of the elastic electrodes increases. At ε_t = 30%, the thickness reduction of the dielectric elastomer only contributes to 3% of the sensor capacitance increase (Figure S1, Supporting Information). A similar response is observed in a soft elastomer dielectric sandwiched between rigid electrodes.[27] Moreover, the surface area of the stretchable gold film electrodes increases by $(1 + \varepsilon_t)(1 - \nu \varepsilon_t)$ when the sensor is stretched by ε_t (Note S1, Supporting Information).[46,47] The effective increase in electrode
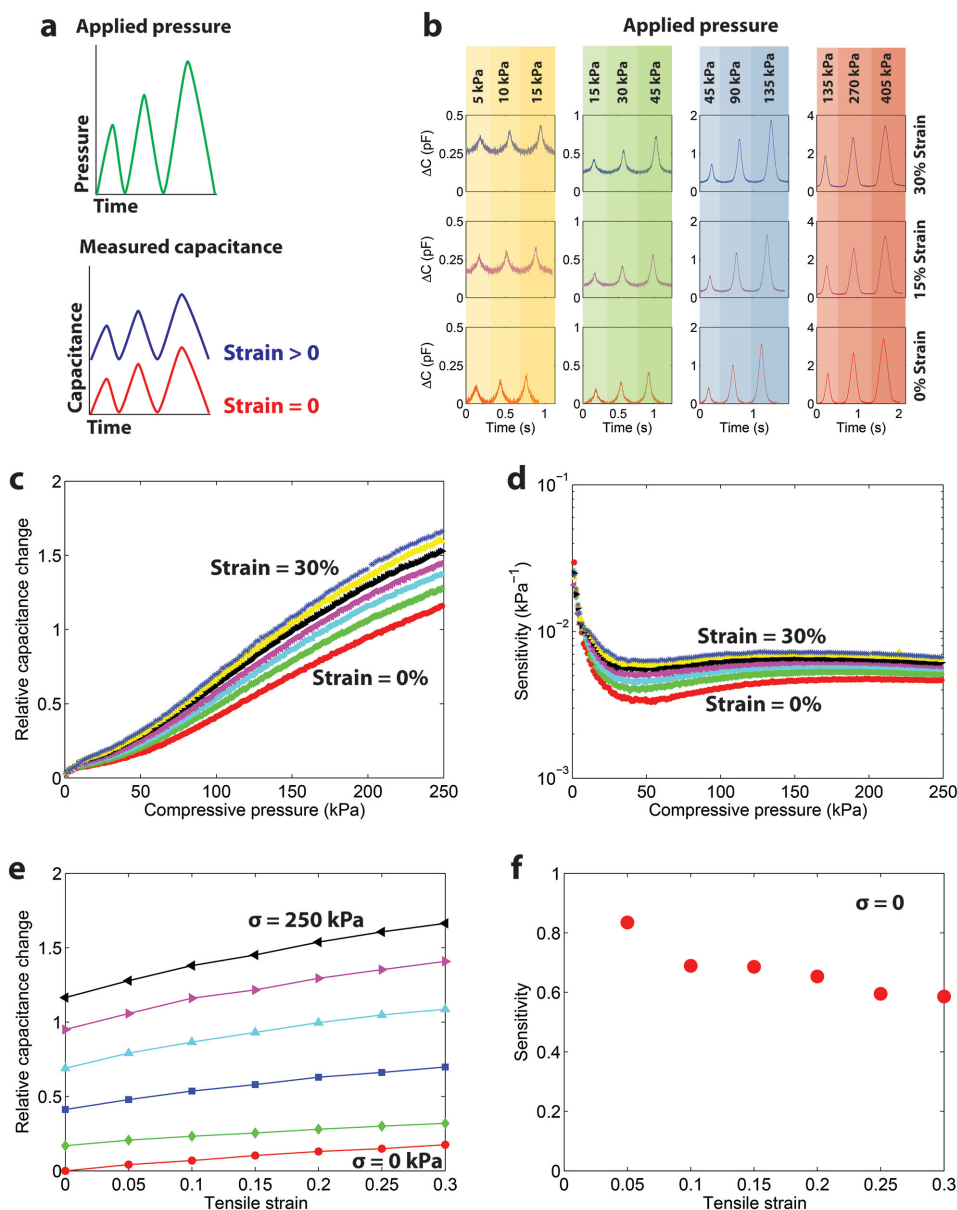
Figure 3. a) During characterization, the applied normal pressure and tensile strains were varied. Increasing the tensile strain ε_t raised the baseline capacitance $C(\sigma = 0, \varepsilon_t)$ while applied pressures σ led to further increases. b) The sensors remained sensitive with applied pressures from 5 to 405 kPa at strain levels of 0%, 15%, and 30% with noticeable contributions to the change in capacitance from both strain and pressure. c) Relative capacitance change over pressures to 250 kPa at tensile strains from 0% to 30% with d) sensitivity at low pressures on the order of 0.01 kPa^{-1} that decays toward a sensitivity on the order of 0.001 kPa^{-1}. e) Relative capacitance change as a function of applied tensile strain at different compressive states (in 50 kPa increments). f) Sensitivity as a function of applied tensile strain ($\sigma = 0$).
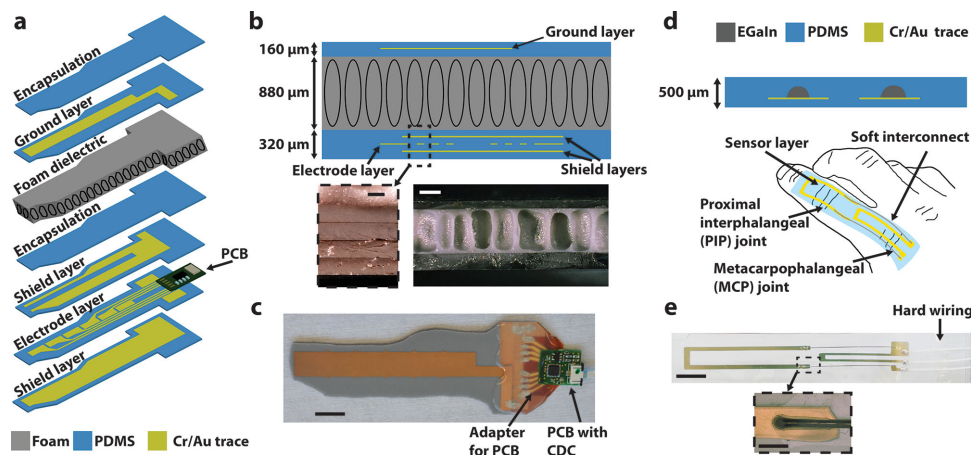
surface area with ε_t leads to a net increase in the sensors compressive pressure sensitivity $(\partial C/C_0)/\partial \sigma$ (Figure 3d).

The pressure sensitivity of these sensors exceeds that of capacitive and resistive devices based on bulk dielectric elastomers,[45,48] (most of which have sensitivities less than 0.001 kPa^{-1}). Alternative foam-like dielectric-based sensors have demonstrated extraordinary pressure sensitivities from 1 Pa^{-1} to 10 kPa^{-1},[13–18,49–52] but rarely combines such performance with macroscopic elasticity or across a wide range of applied pressure. In comparison, the silicone foam sensors maintain stable sensitivity in the 5 to 405 kPa pressure range and when stretched to tens of percent strain.

2.3. Integration of Soft Pressure and Strain Sensors in a Wearable Electronic Skin

Adoption of the soft sensor technology for electronic skin applications requires integration of arrays of soft sensors distributed over large surface areas. Furthermore, the sensors should display

Materials
Views
www.MaterialsViews.com

ADVANCED
FUNCTIONAL
MATERIALS
www.afm-journal.de

FULL PAPER

Figure 4. a) Exploded view of the multilayer capacitive sensors. b) Cross-sectional schematic of the pressure sensor skin with a close-up photograph of the metallized layers and a photograph of the full cross-section. Scale bar on close-up of the metallized layers is 80 μm. Scale bar on the cross-section of the full device is 500 μm. c) Image showing the six stretchable sensors and integrated electronics. Scale bar is 1 cm. d) Schematic of the cross-section and graphical representation on a finger of the resistive flexion sensors for finger bending state information. e) Image showing the fabricated strain and bending sensor. Scale bar on full device is 5 mm. Scale bar on close-up of Au and EGaIn intersection is 1 mm.

maximal signal-to-noise ratio and minimal cross-sensitivities to alternative excitations including temperature and electromagnetic interferences. We sensorized a glove with pressure and flexion sensing strips mounted on the palmar (grasping) and dorsal (back) sides of each finger, respectively (Figure 1). Six capacitive sensors (9 mm × 5 mm nodes, each separated by a 1 mm gap) cover the entire length of the finger (**Figure 4**a–c). Two flexion sensors wrap the metacarpophalangeal (MCP) finger joint (first joint from palm) and proximal interphalangeal (PIP) finger joint (second joint from palm) (Figure 4d,e).

Capacitive sensors electrodes are interfaced with a capacitance-to-digital converter (CDC), and shielded in a metal film-elastomer multilayered construct, prepared thin enough not to impede finger movement (Figure 4c). Pressure- sensing strips consist of four metallized (5/40 nm chromium/gold (Cr/Au) films) 80-μm-thick PDMS layers, an 880-μm-thick silicone foam membrane, and two 80-μm-thick PDMS encapsulation layers (Figure 4a). Brief exposure to oxygen plasma ensures covalent bonding of the silicone membranes (Figure 4b). The soft metallic shields enable reliable contact and pressure discrimination using a finger and metallic and plastic objects (Figure S2,S3, Supporting Information). The noise level in each capacitive sensor does not exceed a few femtofarads (<1% of the initial sensor capacitance) and is stable over prolonged periods (Figure S4, Supporting Information).

Resistive flexion sensor strips provide information on the finger joints position and are used to compensate for the capacitive sensors cross-sensitivity to compression and tension. Each flexion strip consists of two strain sensors (Figure 4d) prepared with highly strain-sensitive stretchable gold and stretchable eutectic gallium indium (EGaIn) liquid metal wiring. The EGaIn was deposited via a pressure-controlled syringe attached to an x-y-z stage, similar in principle to previous work.[53–55] This enables integration of low-resistivity stretchable liquid metal interconnects and high-resistivity stretchable thin-film strain gauges.[56] The EGaIn displays an initial resistance of approximately 1 Ω and negligible resistance change with strain

compared to that of the stretchable gold segments. The process is also potentially compatible with microchannel-based methods of patterning liquid metals, though this was not explored.[34,37,57,58]

The sensor skins, and in particular the capacitive arrays, can be batch-produced on a wafer scale. Reproducibility of the sensors initial capacitance and sensitivity is remarkable (Figure S5–S7, Supporting Information). The soft sensors sustained 250 000 compression cycles (6 Hz, 8 kPa), with increases of only 2.9% and 4.9% in the relative capacitance change ($\Delta C/C_0$) with pressure removed and applied, respectively (Figure S6, Supporting Information). Stretchable thin films of gold on PDMS are extremely robust to cyclic mechanical loading withstanding up to a million cycles to 45% strain.[46,59] The sensor response after 100 cycles to 20% tensile strain remains stable (Figure S7, Supporting Information). The sensors also demonstrate negligible drift over time across all six nodes (0.001% average relative capacitance change per minute, $\sigma = 5.4 \times 10^{-5}$, $n = 6$ sensors) (Figure S4, Supporting Information).

Multi-touch and dynamic surface detection are additional exciting features of the soft electronic skin (Figure S8, Supporting Information). This allows for detecting multiple contact points, necessary when grasping objects with complex contours, and for detecting motion of objects along the surface (Figure S8c, Supporting Information). Connecting several arrays of sensors allows for coverage of large areas, such as an entire hand and arm, and is limited only by the interface electronics (Figure S9, Supporting Information). The resistive flexion sensors expectedly drift with temperature (Figure S10, Supporting Information) as the elastomer significantly expands upon heating (the coefficient of thermal expansion of PDMS is 310 ppm °C−1).[60] The capacitive pressure sensors prepared with low density and anisotropic silicone foam are remarkably temperature insensitive in the 25 °C to 105 °C temperature range (Figure S11, Supporting Information). The relative capacitance increases at a rate of 0.045% per degree from 25 °C to 57 °C and decreases at a rate of 0.33% per degree from 57 °C
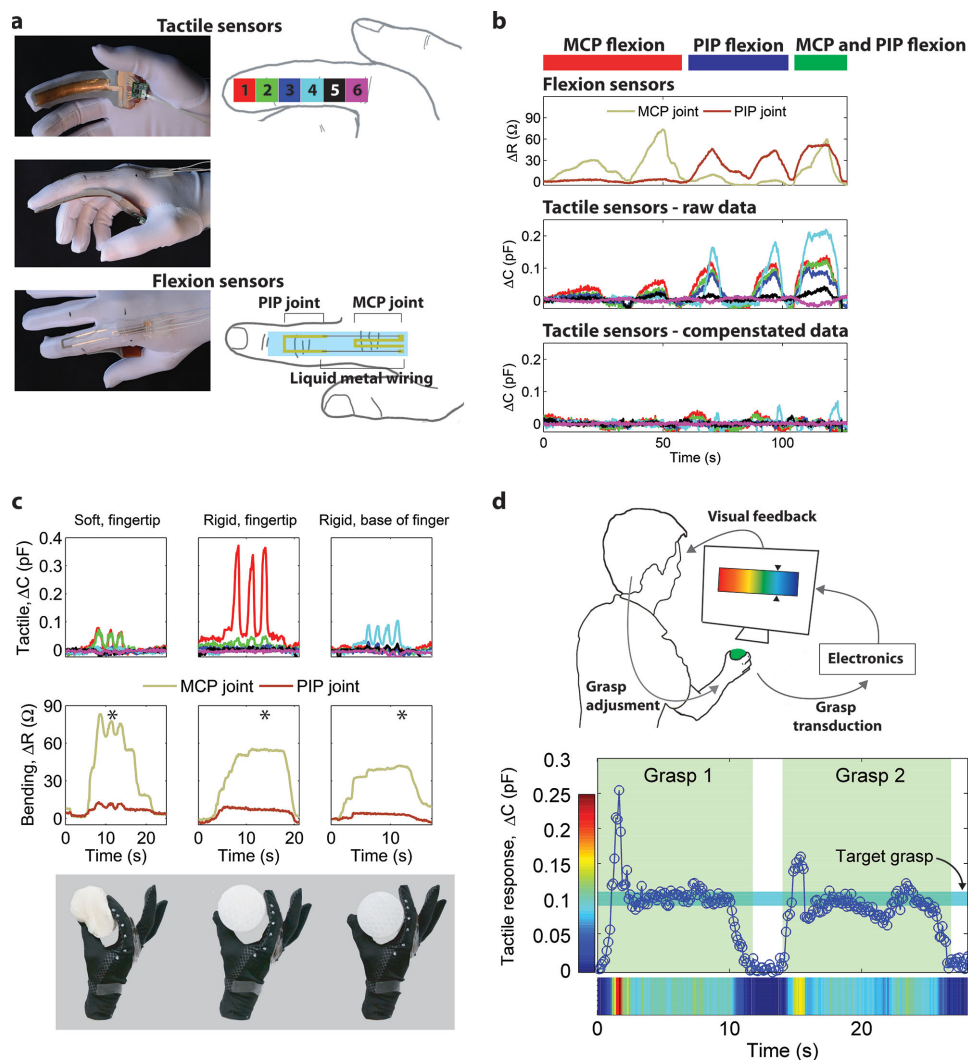
Figure 5. a) Images of the pressure sensors on the palmar side of the hand and flexion sensors on the dorsal side of the hand with schematic representations of the sensor locations on the finger. b) During finger articulation, the strain–pressure cross-sensitivity of the tactile sensors was compensated with the strain sensor response. The three plots show the flexion sensor data, the raw data from the tactile sensors, and the compensated response of the tactile sensors. Data from all six of the capacitive sensors are shown, with the plotted colors representing the corresponding location in the schematic of the finger in Figure 5a. c) Grasps of a soft, compressible object and a rigid, incompressible object of the same diameter. The * symbols denote the time of the images of the grasps at the bottom. d) Tactile response during a grasp and manipulation task demonstrating the wearer was able to adjust the grasp strength to the target pressure during two trials.

to 110 °C. Sensor electrode design may be further customized using lithography techniques and scaled to even larger areas, e.g., the hand palm.

The smart tactile glove provides six pressure sensors and two flexion sensors positioned along the index finger and interfaced to miniaturized PCBs (**Figure 5**a). Strain and tactile information is acquired simultaneously at a sampling rate between 20 to 90 Hz. Improved electronics, for example in an embedded system, would allow for increasing the sampling rate to over 200 Hz for all nodes, the limit of the capacitance-to-digital converter with six nodes. When the finger moves, both flexion and tactile sensors are activated (Figure 5b). The flexion sensor skin reliably discriminates the PIP and MCP joint movement (Figure S12, Supporting Information). The joints angular positions were measured during an arbitrary finger movement. The

root-mean-square (RMS) error was 1° for the PIP joint and 8° for the MCP joint when compared to optical measurements ($n = 10$ samples). Flexion of the finger is also detected with the capacitive sensors. When the finger is closed, the recorded capacitance change is similar to a 50 kPa tactile compression, a significant error if left uncompensated. Advanced calibration to allow for live bending compensation is then performed on each tactile node. During movement of the finger, the response of the capacitive sensors is then corrected as:

$$\Delta C(\sigma) = \Delta C - \Delta C(\Delta R_{MCP}, \Delta R_{PIP}) \quad (1)$$

where ΔC is the raw data, and $\Delta C(\Delta R_{MCP}, \Delta R_{PIP})$ is the compensating capacitive value defined at the selected finger MCP and PIP joints position. Live compensation during finger flexion

Materials
Views
www.MaterialsViews.com

ADVANCED
FUNCTIONAL
MATERIALS
www.afm-journal.de

only is illustrated Figure 5b. Small variations of the capacitive sensors are still noticeable, demonstrating the complexity of finger articulation, but are now negligible compared to tactile stimulation of the sensors.

2.4. Functional Sensing: Object Stiffness Discrimination and Grasping Adjustment

We then investigated the possibility of distinguishing soft from hard objects with the smart tactile glove. During this experiment, objects with distinct compliance were held between the index and thumb, and squeezed three times. The soft and hard objects are both 6.5 cm diameter cylinders prepared with compressible polyurethane foam and rigid plastic, respectively. The combined readouts of the flexion and capacitive sensors differentiate objects stiffness. When squeezing the soft cylinder, pressure and flexion sensor responses increase simultaneously as the soft object is compressed. Conversely, the flexion sensor readout remains constant once the hard object is grasped, and only the capacitive sensors detect the three additional squeezes. Holding the hard object at the base of the fingers (Figure 5c-right), as opposed to the fingertip (Figure 5c-middle) leads to distinct absolute sensor readouts, and highlights the necessity for full-finger coverage in order to gain complete comprehension of the grasp dynamics.

We then evaluated the smart tactile glove in a more complex grasping task using human-in-the-loop visual feedback (Figure 5d). The glove wearer was asked to grasp an object while watching a color on a display. The color represented the tactile information from no touch (dark blue) to high compressing touch (red) with graded intermediate levels. The user was instructed to pick up the object and then adjust his grasp to a pre-set, arbitrarily selected pressure (matching the cyan color on the scale). Visual feedback, in the form of a color (Figure 5d-bottom), of the instantaneous response of the tactile sensors was used to adjust and reach the target contact pressure. Two successive grasps and releases are illustrated Figure 5d. When the object is grabbed, the applied pressure overshoots then decreases and is held at the desired level based on the visual, color feedback. The sensors response time is fast enough to enable a natural manipulation and grasping (Figure S13, Supporting Information). This type of task is critical in robotic and prosthetic applications where robotic control, sensing, actuation, and neural stimulation should be precisely coordinated.[4,61]

3. Conclusion

We have demonstrated a multifunctional, wearable electronic skin, optimized for hand tactile information encoding. Elastic metallization and bulk and foam silicone elastomers are processed with standard fabrication techniques to form a highly compliant and large-area sensory skin conveying live pressure and proprioceptive-like information. Systematic electromechanical characterization of individual and arrayed tactile sensors illustrates the reliability for the soft sensor technology. The integration of flexion and pressure sensors on the dorsal and palmar side of the hand enables combined detection of tactile inputs as well as decoupling of multi-axial stimulation of the soft sensors. The smart tactile glove is robust enough to be worn by humans but also over mechanical prosthetic hands and humanoid robots.[62] We anticipate that this soft technology will open up exciting opportunities in neuroprosthetic research and rehabilitation therapies.

4. Experimental Section

Elastomer Preparation and Characterization: PDMS (Sylgard 184, Dow Corning) was prepared according to manufacturer suggested process by mixing the base and curing agent at a 10:1 weight ratio. Two-part Ecoflex 00-10 (Smooth-On) was mixed at a 1:1 A:B weight ratio. Sub-millimeter thick silicone membranes were prepared by spin-coating on silicon wafers treated with a silane anti-adhesion layer (trichloro(1*H*,1*H*,2*H*,2*H*-perfluorooctyl)silane, Sigma–Aldrich). After 2 h curing at 80 °C, the membranes were then peeled from the wafers and cut to size for testing. The polyurethane (Poron 4701-30-25031-04, Rogers Corporation) and the silicone (Bisco HT800, Rogers Corporation) foam membranes were used as provided. Compression tests were performed with an Electromechanical Universal Test System (UTS) (C42.503, MTS Systems). All tested samples had a thickness of approximately 0.8 mm. Samples were placed on top of a large, flat plate covered with a polyimide foil and compressed with a teflon-coated circular indenter with a diameter of 1 cm (indenter diameter about 12× sample thickness). Lateral dimensions of the samples were maintained at more than 2× the diameter of the indenter. Tension tests were performed on a customized uniaxial stretching setup driven by a brushless rotary servomotor (BMS60-UFA, Aerotech) with a 1500 g load cell (UF1, LCM Systems) and inductive position sensors (Li200P0-Q25LM0, Turck). The motor drives a threaded rod that interfaces with the sample holders and is controlled with a custom LabView code. Samples for tension tests had a rectangular shape with approximately 0.8 mm thickness, 10 mm width, and 16 mm length, and were clamped on either end.

Integrated Pressure Sensor Array Fabrication: PDMS was prepared in a Thinky Mixer then spun on a silane-treated silicon wafer at 1250 RPM for 30 s in a spin coater (SCS 6800, Specialty Coating Systems) and cured at 80 °C for 2 h. The PDMS was subsequently metallized by evaporating 5/40 nm chromium/gold bilayers through a shadow mask (Auto 306 thermal evaporator). Multiple PDMS layers were bonded sequentially, from the bottom up, after a 25 s exposure to an oxygen plasma (PDC-32G-2 etcher, Harrick Plasma). A layer of ethanol was used to delay creation of covalent bonds and allow for alignment of the stacked layers, and afterwards the ethanol was allowed to evaporate for at least 12 h between each bonding step. The silicone foam layer was bonded using the same process. When required, metallized layers were electrically interconnected with a silver-epoxy composite (H27D, EPO-TEK). Custom read-out PCBs were bonded with anisotropic conductive tape (9705 Transfer Tape, 3 M) on a 127-μm-thick polyimide sheet (200HN Kapton, DuPont) carrying sputtered 10/50 nm chromium/gold metallic contact pads (DP 650, Alliance-Concept). Stretchable metal traces on the elastomer were manually connected to the metallic pads on the polyimide sheet with the H27D silver composite. The PCB-polyimide adapter was then fully encapsulated in a silicone sealant (734, Dow Corning).

Single Pressure Sensor Node Fabrication: Single-node pressure sensors were prepared using the same process steps but only two chromium/gold metallized PDMS layers were used to form parallel-plate capacitors.

Flexion Sensors: Chromium/gold (5/40 nm) bilayers were thermally evaporated onto a 125-μm-thick PDMS substrate following identical procedure to pressure sensors fabrication. Liquid metal wires (eutectic gallium indium, EGaIn, Sigma–Aldrich) were then printed on the PDMS membrane using a syringe loaded with EGaIn attached to a precision x-y-z stage (GIX Microplotter II, Sonoplot) and held about 70 μm above

the substrate. A controlled pressure (1–5 kPa) was applied in the syringe (TS250, OK International) while it was moved at 200 µm s^{-1} in the x–y plane to draw the liquid metal lines.[56] The elastic wires were next connected to Teflon-coated silver wires for interfacing with readout electronics. Then, the sensors on PDMS were encapsulated with a thin layer of PDMS spun at 250 RPM and cured at 60 °C in an oven (UFE 500, Memmert).

Assembly of Pressure and Flexion Sensor Strips on a Textile Glove: Soft sensing strips were mounted onto a textile glove with a thin layer of Ecoflex 00-10, which was cured at 50 °C in an oven (UFE 500, Memmert).

Single-Node Characterization: An LCR meter (E4980A, Agilent) was used to monitor the capacitance of the single-node sensors under applied strains and pressures. Tests of the sensors under dynamic tensile strain were performed with a custom uniaxial stretcher. Tests of the sensors under both strain and pressure were performed using a manual stretcher to apply static strains while the UTS was used to apply dynamic pressures.

Integrated Pressure Sensors Array and Strain Sensor Characterization: A 16-bit capacitance-to-digital converter (AD7147, Analog Devices) was used to convert the sensor capacitance levels to a digital signal. The resistance of the strain sensors was measured by monitoring the voltage across a 5 kΩ reference resistor in a 1.2 V voltage divider with a 16-bit analog-to-digital converter (ADS1115, Texas Instruments). All of the electronics were assembled on custom PCBs. Custom MATLAB code was interfaced with the PCBs over a serial connection (Bus Pirate, Dangerous Prototypes).

Reliability Tests: Tests of the sensors under cyclic pressure were performed at 6 Hz with a custom setup including a solenoid (KLMSB 30 Z, Magnet AG) driven by a function generator (33210A, Agilent). Cyclic tension tests were performed with a custom uniaxial stretcher.

Thermal Tests: Tests of the thermal stability were performed in an oven (B180, Nabertherm) while the temperature was monitored with a bandgap temperature sensor (MCP9808, Microchip).

Supporting Information

Supporting Information is available from the Wiley Online Library or from the author.

Acknowledgements

[1] A. Gallace, C. Spence, *In Touch with the Future: the Sense of Touch from Cognitive Neuroscience to Virtual Reality*, Oxford University Press, Somerville College, Oxford, UK **2014**.

[2] A. E. Saddik, M. Orozco, M. Eid, J. Cha, in *Haptics Technology: Bringing Touch to Multimedia*, (Eds: M. Ferre, M. O. Ernst, A. Wing), Springer-Verlag, Berlin, Heidelberg **2011**, Ch. 1.

[3] R. S. Dahiya, G. Metta, M. Valle, G. Sandini, *IEEE Trans. Robotics* **2010**, *26*, 1.

[4] S. Raspopovic, M. Capogrosso, F. M. Petrini, M. Bonizzato, J. Rigosa, G. Di Pino, J. Carpaneto, M. Controzzi, T. Boretius, E. Fernandez, G. Granata, C. M. Oddo, L. Citi, A. L. Ciancio, C. Cipriani, M. C. Carrozza, W. Jensen, E. Guglielmelli, T. Stieglitz, P. M. Rossini, S. Micera, *Sci. Transl. Med.* **2014**, *6*, 222ra19.

[5] F. Tremblay, K. Wong, R. Sanderson, L. Cote, *Somatosensory Motor Res.* **2003**, *20*, 127.

[6] M. M. Merzenich, W. M. Jenkins, *J. Hand Therapy* **1993**, *6*, 89.

[7] J. Konczak, A. Sciutti, L. Avanzino, V. Squeri, M. Gori, L. Masia, G. Abbruzzese, G. Sandini, *Brain* **2012**, *135*, 3371.

[8] M. L. Hammock, A. Chortos, B. C.-K. Tee, J. B.-H. Tok , Z. Bao, *Adv. Mater.* **2013**, *25*, 5997.

[9] S. Bauer, S. Bauer-Gogonea, I. Graz, M. Kaltenbrunner, C. Keplinger, R. Schwödiauer, *Adv. Mater.* **2014**, *26*, 149.

[10] Y. Hattori, L. Falgout, W. Lee, S.-Y. Jung, E. Poon, J. W. Lee, I. Na, A. Geisler, D. Sadhwani, Y. Zhang, Y. Su, X. Wang, Z. Liu, J. Xia, H. Cheng, R. C. Webb, A. P. Bonifas, P. Won, J.-W. Jeong, K.-I. Jang, Y. M. Song, B. Nardone, M. Nodzenski, J. A. Fan, Y. Huang, D. P. West, A. S. Paller, M. Alam, W.-H. Yeo, J. A. Rogers, *Adv. Healthcare Mater.* **2014**, *3*, 1597.

[11] M. Kaltenbrunner, T. Sekitani, J. Reeder, T. Yokota, K. Kuribara, T. Tokuhara, M. Drack, R. Schwödiauer, I. Graz, S. Bauer-Gogonea, S. Bauer, T. Someya, *Nature* **2013**, *499*, 458.

[12] L. Xu, S. R. Gutbrod, A. P. Bonifas, Y. Su, M. S. Sulkin, N. Lu, H.-J. Chung, K.-I. Jang, Z. Liu, M. Ying, C. Lu, R. C. Webb, J.-S. Kim, J. I. Laughner, H. Cheng, Y. Liu, A. Ameen, J.-W. Jeong, G.-T. Kim, Y. Huang, I. R. Efimov, J. A. Rogers, *Nat. Commun.* **2014**, *5*, 3329.

[13] J. Park, Y. Lee, J. Hong, M. Ha, Y.-D. Jung, H. Lim, S. Y. Kim, H. Ko, *ACS Nano* **2014**, *8*, 4689.

[14] B. Zhu, Z. Niu, H. Wang, W. R. Leow, H. Wang, Y. Li, L. Zheng, J. Wei, F. Huo, X. Chen, *Small* **2014**, *10*, 3625.

[15] Q. Shao, Z. Niu, M. Hirtz, L. Jiang, Y. Liu, Z. Wang, X. Chen, *Small* **2014**, *10*, 1466.

[16] S. Gong, W. Schwalb, Y. Wang, Y. Chen, Y. Tang, J. Si, B. Shirinzadeh, W. Cheng, *Nat. Commun.* **2014**, *5*, 3132.

[17] L. Pan, A. Chortos, G. Yu, Y. Wang, S. Isaacson, R. Allen, Y. Shi, R. Dauskardt, Z. Bao, *Nat. Commun.* **2014**, *5*, 3002.

[18] G. Schwartz, B. C.-K. Tee, J. Mei, A. L. Appleton, D. H. Kim, H. Wang, Z. Bao, *Nat. Commun.* **2013**, *4*, 1859.

[19] S. Park, H. Kim, M. Vosgueritchian, S. Cheon, H. Kim, J. H. Koo, T. R. Kim, S. Lee, G. Schwartz, H. Chang, Z. Bao, *Adv. Mater.* **2014**, *26*, 7324.

[20] C.-L. Choong, M.-B. Shim, B.-S. Lee, J. Jeon, D.-S. Ko, T.-H. Kang, J. Bae, S. H. Lee, K.-E. Byun, J. Im, Y. J. Jeong, C. E. Park, J.-J. Park, U.-I. Chung, *Adv. Mater.* **2014**, *26*, 3451.

[21] M. H. Lee, *Int. J. Robotics Res.* **2000**, *19*, 636.

[22] S. A. Mascaro, H. H. Asada, *IEEE Trans. Robotics Automation* **2001**, *17*, 698.

[23] V. E. Abraira, D. D. Ginty, *Neuron* **2013**, *79*, 618.

[24] K. Fukuda, Y. Takeda, Y. Yoshimura, R. Shiwaku, L. T. Tran, T. Sekine , M. Mizukami, D. Kumaki, S. Tokito, *Nat. Commun.* **2014**, *5*, 4147.

[25] G. A. Salvatore, N. Münzenrieder, T. Kinkeldei, L. Petti, C. Zysset, I. Strebel, L. Buthe, G. Troster, *Nat. Commun.* **2014**, *5*, 2982.

[26] C. Wang, D. Hwang, Z. Yu, K. Takei, J. Park, T. Chen, B. Ma, A. Javey, *Nat. Mater.* **2013**, *12*, 899.

[27] M. Ying, A. P. Bonifas, N. Lu, Y. Su, R. Li, H. Cheng, A. Ameen, Y. Huang, J. A. Rogers, *Nanotechnology* **2012**, *23*, 344004.

[28] A. Schmitz, P. Maiolino, M. Maggiali, L. Natale, G. Cannata, G. Metta, *IEEE Trans. Robotics* **2011**, *27*, 389.

[29] Tekscan, *Grip System for R&D tactile grip force and pressure measurement*, http://www.tekscan.com/grip-pressure-measurement (accessed: May **2014**).

[30] G. Buscher, R. Koiva, C. Schurmann, R. Haschke, H. J. Ritter, *IEEE/ RAS Int. Conf. on Humanoid Robots*, Osaka, Japan **2012**, p 204.

FULL PAPER

[31] *Pressure Profile Systems: Stretchable TactArray System*, http://www.pressureprofile.com/s/Stretchable-TactArray-System.pdf (accessed: September **2014**).

[32] T. Barois, L. Tadrist, C. Quilliet, Y. Forterre, *Phys. Rev. Lett.* **2014**, *113*, 214301.

[33] N. Stubler, J. Fritzsche, M. Kluppel, *Polym. Eng. Sci.* **2011**, *51*, 1206.

[34] Y.-L. Park, B.-R. Chen, R. J. Wood, *IEEE Sens. J.* **2012**, *12*, 2711.

[35] J.-B. Chossat, Y.-L. Park, R. J. Wood, V. Duchaine, *IEEE Sens. J.* **2013**, *13*, 3405.

[36] F. L. Hammond III, Y. Mengüç, R. J. Wood, *IEEE/RSJ Int. Conf. on Intelligent Robots and Systems,* Chicago, IL, USA **2014**, p 4000.

[37] Y. Mengüç, Y.-L. Park, H. Pei, D. Vogt, P. M. Aubin, E. Winchell, L. Fluke, L. Stirling, R. J. Wood, C. J. Walsh, *Int. J. Robotics Res.* **2014**, *33*, 1748.

[38] F. Lorussi, S. Galatolo, R. Bartalesi, D. De Rossi, *IEEE Sens. J.* **2013**, *13*, 217.

[39] J. Kim, M. Lee, H. J. Shim, R. Ghaffari, H. R. Cho, D. Son, Y. H. Jung, M. Soh, C. Choi, S. Jung, K. Chu, D. Jeon, S.-T. Lee, J. H. Kim, S. H. Choi, T. Hyeon, D.-H. Kim, *Nat. Commun.* **2014**, *5*, 5747.

[40] M. F. Ashby, *Metall. Trans. A* **1983**, *14*, 1755.

[41] C. H. Daly, G. F. Odland, *J. Invest. Dermatol.* **1979**, *73*, 84.

[42] D. J. Lipomi, M. Vosgueritchian, B. C.-K. Tee, S. L. Hellstrom, J. A. Lee, C. H. Fox, Z. Bao, *Nat. Nanotechnol.* **2011**, *6*, 788.

[43] S. Yao, Y. Zhu, *Nanoscale* **2014**, *6*, 2345.

[44] D. P. J. Cotton, I. M. Graz, S. P. Lacour, *IEEE Sens. J.* **2009**, *9*, 2008.

[45] D. P. J. Cotton, I. M. Graz, S. P. Lacour, *Procedia Chem.* **2009**, *1*, 152.

[46] I. M. Graz, D. P. J. Cotton, S. P. Lacour, *Appl. Phys. Lett.* **2009**, *94*, 071902.

[47] S. Wagner, S. P. Lacour, J. Jones, P.-H. I. Hsu, J. C. Sturm, T. Li, Z. Suo, *Phys. E* **2004**, *25*, 326.

[48] Y.-L. Park, C. Majidi, R. Kramer, P. Berard, R. J. Wood, *J. Micromech. Microeng.* **2010**, *20*, 125029.

[49] J. Park, Y. Lee, J. Hong, Y. Lee, M. Ha, Y. Jung, H. Lim, S. Y. Kim, H. Ko, *ACS Nano* **2014**, *8*, 12020.

[50] C. Pang, G.-Y. Lee, T.-I. Kim, S. M. Kim, H. M. Kim, S.-H. Ahn, K.-Y. Suh, *Nat. Mater.* **2012**, *11*, 795.

[51] S. Jung, J. H. Kim, J. Kim, S. Choi, J. Lee, I. Park, T. Hyeon, D.-H. Kim, *Adv. Mater.* **2014**, *26*, 4825.

[52] H.-K. Lee, S.-I. Chang, E. Yoon, *J. Microelectromech. Syst.* **2006**, *15*, 1681.

[53] J. W. Boley, E. L. White, G. T.-C. Chiu, R. K. Kramer, *Adv. Funct. Mater.* **2014**, *24*, 3501.

[54] C. Ladd, J.-H. So, J. Muth, M. D. Dickey, *Adv. Mater.* **2013**, *25*, 5081.

[55] J. T. Muth, D. M. Vogt, R. L. Truby, Y. Mengüç, D. B. Kolesky, R. J. Wood, J. A. Lewis, *Adv. Mater.* **2014**, *26*, 6307.

[56] H. O. Michaud, J. Teixidor, S. P. Lacour, *IEEE Int. Conf. Micro Electro Mechanical Systems,* Estoril, Portugal **2015**, p 760.

[57] R. K. Kramer, C. Majidi, R. Sahai, R. J. Wood, *IEEE/RSJ Int. Conf. on Intelligent Robots and Systems,* San Francisco, CA, USA **2011**, p 1919.

[58] M. D. Dickey, R. C. Chiechi, R. J. Larsen, E. A. Weiss, D. A. Weitz, G. M. Whitesides, *Adv. Funct. Mater.* **2008**, *18*, 1097.

[59] I. R. Minev, P. Musienko, A. Hirsch, Q. Barraud, N. Wenger, E. M. Moraud, J. Gandar, M. Capogrosso, T. Milekovic, L. Asboth, R. F. Torres, N. Vachicouras, Q. Liu, N. Pavlova, S. Duis, A. Larmagnac, J. Vörös, S. Micera, Z. Suo, G. Courtine, S. P. Lacour, *Science* **2015**, *347*, 159.

[60] M.-J. Jiang, Z.-M. Dang, H.-P. Xu, *Appl. Phys. Lett.* **2006**, *89*, 182902.

[61] D. W. Tan, M. A. Schiefer, M. W. Keith, J. R. Anderson, D. J. Tyler, *Sci. Transl. Med.* **2014**, *6*, 257ra138.

[62] A. P. Gerratt, N. Sommer, S. P. Lacour, A. Billard, *IEEE/RSJ Int. Conf. on Humanoid Robots,* Madrid, Spain **2014**, p 238.